Absolute magnetometry with ³He

Midhat Farooq¹, Timothy Chupp¹, Joe Grange^{1,2}, Alec Tewsley-Booth¹,
David Flay³, David Kawall³, Natasha Sachdeva¹, Peter Winter²

¹Physics Department, University of Michigan, Ann Arbor, MI 48109 USA

²Argonne National Laboratory, Lemont, IL 60439 USA

³Physics Department, University of Massachussetts, Amherst, MA 01003 USA

(Dated: June 2, 2020)

We report development of a highly accurate (ppb) absolute magnetometer based on 3 He NMR. Optical pumping polarizes the spins, long coherence times provide high sensitivity, and the 3 He electron shell effectively isolates the nuclear spin providing accuracy limited only by corrections for materials, sample shape and magnetization. Our magnetometer was used to confirm calibration, to 32 ppb, of the magnetic-field sensors used in recent measurements of the muon magnetic moment anomaly $(g_{\mu}-2)$, which differs from the Standard Model by 2.4 ppm. With independent determination of the magnetic moment of 3 He, this work will lead the way to a new absolute magnetometry standard.

Magnetometry, determining the intensity of a magnetic field over space and time, is crucial to many fields of applied and fundamental science including medicine, materials science, geology and geodesy, astronomy and fundamental physics. Often competing magnetometry requirements include sensitivity, stability, absolute accuracy, bandwidth and spatial resolution, and many applications require accurately determining the magnetic field intensity in Tesla (kg \cdot s⁻² \cdot A⁻¹). The most sensitive magnetometers, superconducting quantum-interference devices (SQUIDs) reach sub fT/\sqrt{Hz} sensitivity [1], but are not absolute. Optically pumped atomic magnetometers approach this sensitivity in small fields [2, 3], but are generally not highly accurate or stable. Accurate absolute magnetometers include rotating coils [4] and calibrated NMR [5].

Magnetic fields are most accurately determined by measuring the frequency corresponding to the energy difference of two quantum states. The frequency ω and magnetic field B are related by $B = \omega \left(\hbar J/|\mu| \right) = \omega/|\gamma|$, where $\hbar J$ is the total angular momentum, μ is the magnetic moment, and $\gamma = \mu/\hbar J$. J = 1/2 nuclei in diamagnetic materials are the most nearly ideal two-state quantum systems, and NMR of proton rich substances, e.g. H₂O, is most commonly encountered. For pure H₂O, the shielded proton magnetic moment for a spherical sample at 25° $\mu'_p(25^\circ)$ is known to 11.3 ppb, limited by measurement of $\mu'_p/\mu_e(H)$ [6, 7].

In practical magnetometry, temperature-dependent sample, shape and external material effects lead to perturbations of the magnetic field that must be calibrated or corrected. With much smaller intrinsic corrections illustrated by the practically engineered magnetometer demonstrated in this paper, a new more precise and more accurate standard for magnetometry can be established with ³He. Unlike H₂O, for which the signal size is proportional to 1/T, the ³He is hyperpolarized by laser optical pumping techniques; thus ³He magnetometry is applicable over a very broad range of magnetic fields using NMR

for fields >0.1 T and atomic sensors for lower fields [8].

Quantities relevant to determining the magnetic moment of a free ³He atom are provided in the Supplement [9]. Diamagnetic shielding of the atomic electrons reduces the field at the ³He nucleus, referred to as the helion. The shielded helion moment μ'_h has been measured to 4.3 ppb relative to the shielded proton magnetic moment in water [10] and to 4 ppb relative to protons in high-pressure H_2 [11], but the uncertainty on μ'_h , 11.4 ppb, is dominated by the uncertainty on $\mu_p'/\mu_e(H)$. To eliminate the proton from the chain, effort is underway [14, 15] to directly measure magnetic moment of the unshielded nucleus μ_h in a Penning trap with techniques similar to those used to measure the proton [16] and antiproton [17] g-factors. The high-precision theoretical calculation of the diamagnetic shielding [18], which is only weakly temperature dependent, would provide the shielded magnetic moment μ_h' at the few ppb level.

The muon magnetic moment anomaly: A spin $\frac{1}{2}$ -particle (lepton) with charge q_l and mass m_l has a magnetic moment $\mu_l = g_l \frac{q_l}{2m_l} \frac{\hbar}{2}$. For a structureless particle with no radiative corrections $g_l=2$ [19], however due to interactions with the virtual fields of the quantum vacuum corrections to $q_l = 2(1 + a_l)$ [20–22]. The largest correction, $\approx 0.1\%$, is due to QED with the strong and weak interactions entering at three and six orders of magnitude less, respectively. For the muon, the most recent Standard Model determinations of a_{μ}^{SM} are summarized in [23, 24]. The muon magnetic-moment anomaly has been measured by producing muons in accelerators at CERN [25] and Brookhaven [26]. The most recent measurements a_{μ}^{exp} from Brookhaven (E821) for μ^{+} [27] and μ^{-} [28] reveal $a_{\mu}^{\rm exp} - a_{\mu}^{\rm SM} = (28.0 \pm 7.4) \times 10^{-10}$ or (2.40 ± 0.63) ppm, using $a_{\mu}^{\rm SM}$ from [24]. A new measurement with higher statistical precision and smaller systematic errors is underway at Fermilab and is expected to improve the uncertainty by a factor of four [29].

Experimentally, muons are confined in a 7.1 m radius magnetic storage ring with weak vertical focusing by elec-

tric quadrupole fields. The anomaly frequency, determined from the variation of the rate of μ decays into positrons or electrons that exceed a threshold energy, is $\omega_{a_{\mu}}\approx a_{\mu}\frac{e}{m_{\mu}}\tilde{B}$ for muon momentum near 3.094 GeV/c, where the electric field effects are effectively cancelled. The field averaged over the muon trajectories and time is $\tilde{B}\approx 1.45~\mathrm{T}$. A chain of measurements using proton-NMR magnetometers (probes) calibrated with high-purity H₂O yields the frequency $\tilde{\omega}_p'=\frac{2|\mu_p'|}{\hbar}\tilde{B}$. In terms of $\omega_{a_{\mu}}$ and $\tilde{\omega}_p'$,

$$a_{\mu} = \frac{g_e}{2} \frac{\omega_{a_{\mu}}}{\tilde{\omega}_p'} \left| \frac{\mu_p'}{\mu_e} \right| \frac{m_{\mu}}{m_e}. \tag{1}$$

where μ'_p/μ_e is determined to 10.5 ppb [9], g_e has been determined to 0.28 ppt [30], and m_{μ}/m_e is determined to 22 ppb from the muonium hyperfine splitting [31] and QED [7]. In this work, the ³He magnetometer independently determined and confirmed the systematic corrections to the standard H₂O reference probes used in E821. The ³He Magnetometer illustrated in Fig. 1 is a compact device designed to operate at 1.45 T providing polarization and NMR magnetometry in-situ. The required elements are the ³He sample contained in a glass cell, coils to excite a discharge in the ³He, the NMR coil for excitation and pickup of free-precession, optical fibers to guide the incident optical pumping light and to monitor transmission through the cell for laser tuning, circular polarization optics, and the mounting structure. The design principles require removing all ferromagnetic materials including electronic components and cables, minimizing materials near the ³He sample and fabricating as closely as possible cylindrically or spherically symmetric distributions of materials.

The magnetometer was assembled in a 3-D printed mount with groves that aligned the components. In our initial (Mark-I) assemblies the mount was polylactic acid thermoplastic (PLA) with a square cross section "clamshell" for ease of mounting, alignment and access for cell orientation and material perturbation studies. The plastic mount was enclosed in 0.002-inch thick copper folded from a flat sheet and soldered at the joints. The ³He cells were blown borosilicate (PYREX) glass, approximately spherical with 2.5 cm diameter and a stem several mm long (see Supplement [9]. Several ³He pressures were investigated, and 10-torr (20°C) provided the best combination of polarization lifetime, free-precession relaxation time (T_2^*) and signal size.

Optical pumping of metastable ³He or MEOP has been extensively studied, most recently at high magnetic fields relevant to this work [9, 32–34]. A discharge was excited by radio frequency (4-6 MHz) applied to a 2-cm-diameter coil pair in contact with the outside of the glass cell. The input fiber provided optical pumping light from a 1083 nm, 2W fiber-amplified laser [35]. For development studies at 2-3 mT an optical polarimeter [36] monitored the

circular polarization of the 668 nm fluorescence indicating 30-50% ³He polarization. We did not directly measure the ³He polarization at 1.45 T, however NMR signal sizes and system parameters were consistent with 4-8% in the 10-torr cell. The polarization (discharge on) time was typically 1-2 minutes, and the polarization lifetime was greater than five hours.

The ³He NMR system consisted of a saddle coil surrounding the ³He cell that produced a field along the y-axis. The NMR coil, matched to 50Ω and tuned to the ³He resonant frequency $\omega_h'/(2\pi) \approx 47.1$ MHz, provided both the NMR pulse and inductive pickup. The coil was connected to the NMR controller described in the Supplement. The mixer reference frequency was set below the precession frequency, and the 100-300 Hz mixed-down signal was digitized. An identical NMR controller for the H₂O probes was tuned to 61.7 MHz and interfaced to the same data acquisition system. The NMR tip angle was $\approx 23^{\circ}$ for ³He leaving about 90% of the longitudinal polarization after each pulse and providing variation of the longitudinal and transverse magnetization for systematic studies. The 90° pulse for H₂O protons maximized the signal size. The pulse and mixer reference frequencies for both the ³He and proton (H₂O) channels and the data acquisition sample trigger were generated by separate function generators all locked to a single rubidium clock. Details of the NMR signal processing are discussed in the Supplement [9].

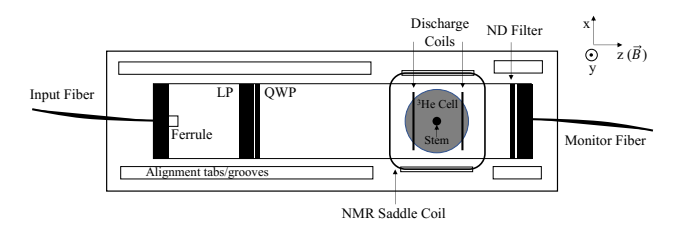


FIG. 1: The ³He magnetometer assembly described in the text. The assembly is 5 cm square in cross section and 15 cm long. The distance from the input-fiber ferrule to the cell is approximately 8 cm. LP and QWP indicate the linear polarizer and quarter wave plate.

Calibration of ³He and E821 H₂O probes: The two H₂O probes used in E821, one with a spherical sample and one with a cylindrical sample, are described in detail in [37]. The calibration of each H₂O probe to ³He used a precision-shimmed superconducting solenoid magnet. The magnetic field drift was dominated by a diurnal cycle and was less than 60 ppb over the five hour calibration measurements. The ³He magnetometer and H₂O probes were mounted on a translation stage, and a positive or negative linear gradient along each axis was applied by rapidly ($\lesssim 1$ min) reversing the gradient-coil currents to determine a unique position (x_0, y_0, z_0), the $\Delta B = 0$ position. Adjusting each probe to find x_0 and y_0 then required only translation along the z axis to position each probe at the $\Delta B = 0$ position indicated in Fig. 2.

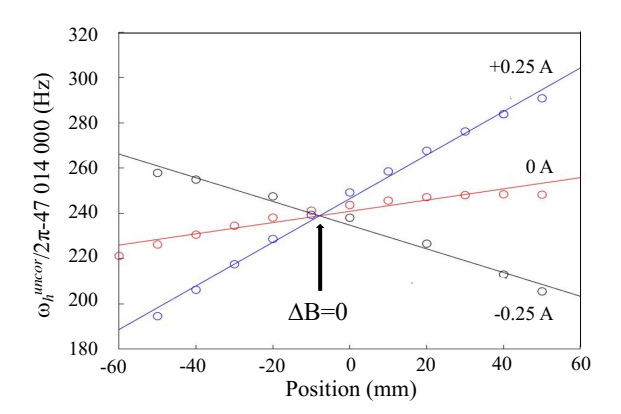


FIG. 2: (Color on line) Scan of the ³He frequency as the magnetometer was translated along z with positive and negative gradient currents showing the $\Delta B = 0$ position z_0 . The solenoid's higher order (quadratic) gradients are evident; straight lines are provided to guide the eye.

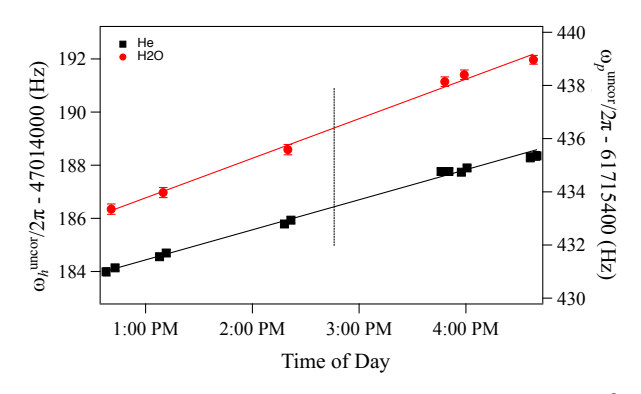


FIG. 3: (Color on line) Uncorrected frequencies for 3 He (left axis) and the spherical H₂O probe (right axis); the solid lines are linear fits vs time. The χ^2_{ν} , 1.0 and 1.2, respectively for 3 He and H₂O, are accounted for in the magnetic drift uncertainties. The vertical dotted line indicates the time to which all frequencies are interpolated. Both scales span 10 Hz. The different slopes are due to the different magnetic moments.

Calibration studies of the two H_2O probes were undertaken on separate days, with small modifications to the 3He setup between the two studies. Fig. 3 shows the uncorrected frequencies ω_3^{uncor} and ω_p^{uncor} as a function of time during calibration of the cylindrical H_2O probe showing the effect of the magnetic-field drfit. All frequency measurements were interpolated to the average time of the 3He measurements indicated by the vertical dotted line in Fig. 3. Corrections were applied to both species' interpolated frequencies to provide the two shielded frequencies ω_3' and ω_p' for each H_2O probe at the specified position and time.

Corrections and uncertainties: Corrections, determined independently within one day of each calibration study, are presented in Table I. Corrections fall into four categories: materials external to the sample, sample container materials, sample-material magnetization effects, and temperature dependence. Though all of these are in

principle applicable to both species, the size and method of determining the corrections differed significantly.

External materials include all components of a probe, cables, translation stage and mounting structure other than the sample and glass sample container. All effects of external materials were measured with an auxiliary vasoline-sample NMR probe at the ΔB = position with/without the ³He sample or H₂O probe. The auxiliary probe temperature was not monitored (temperature dependence 2.5 ppb/° C [38]) and uncertainties including those due to temperature variations were estimated from the scatter of multiple measurements. Due to the NMR coil inhibiting positioning of the auxiliary probe at the exact position of the ³He cell, and because the $\Delta B = 0$ positioning could not be checked with the ³He cell removed, the auxiliary probe was moved back and forth a few mm over cell position to estimate the uncertainty due to position misalignment.

For the H_2O probe ± 10 ppb variations when rotating the probe around the probe axis were reported by [37] and confirmed for this work. Rotations of the stem with respect to the axis of the magnet with polar angle $\theta=0$ and 90° and with ϕ =0 and 90° were consistent with modeling the stem as a magnetic dipole, which predicted $P_2(\cos\theta)$ dependence at the cell center. For the H₂O calibration measurements, the stem was oriented along y $(\theta = 90^{\circ})$; extrapolating to the magic angle $\theta = 54^{\circ}$ resulted in the correction of -0.61 ± 0.20 Hz. The stem also caused magnetic gradients, which resulted in a factor of two shorter T_2^* with $\theta = 0^\circ$. Rotation of the cell around the stem axis showed variations of 0.35 Hz, included as an uncertainty. The same ³He cell and stem orientation corrections were applied to both H₂O probes. In principle, there was also a correction for the different displacement of air ($\approx 20\%$ paramagnetic O_2) by the sample and the auxiliary probe. For a spherical ³He sample, this effect would vanish. Modeling the air displaced by the stem as a dipole, the magnetic field at the center of the cell has an amplitude less than about 20 fT. For the H₂O probes, the sample was not removed, and there was no correction.

Sample magnetization dependence arises due to magnetic susceptibility and due to ³He nuclear polarization. For perfectly spherical samples the average long-range contribution to the field anywhere in the sample vanishes [39]. Modeling the hyperpolarized ³He gas in the stem as a magnetic dipole predicts ≈ 0.5 pT for 10% ³He polarization, corresponding to a shift less than 15 μ Hz. The H₂O shape correction is given by $\delta_{\rm shape} = -\Delta \omega_p'/\omega_p' = \chi^{\rm H_2O}(T)(\epsilon-1/3)$ (SI units), where $\chi^{\rm H_2O}(T)$ is the susceptibility. For an infinitely-long cylinder perpendicular to \vec{B} , $\epsilon=1/2$ and $\Delta\omega_p'=93.10$ Hz; for a sphere, $\epsilon=1/3$. Additional magnetization-dependent shifts have been revealed in recent studies with hyperpolarized ³He-¹²⁹Xe mixtures used in a comagnetometer configuration [40–43]. Scaling these effects from [44] suggests shifts much

	Spherical H ₂ O (Hz)			Cylindrical H ₂ O (Hz)				
	$_{\mathrm{H_2O}}$		³ He		H_2O		3 He $^{'}$	
Source	Corr.	Unc.	Corr.	Unc.	Corr.	Unc.	Corr.	Unc.
External materials	10.61	0.49	21.38	1.22	13.82	0.49	23.64	1.13
Probe materials	2.71	0.62	-	-	2.90	0.62	-	-
H ₂ O Probe-material asymmetry*	0	1.24	-	-	0	1.24	-	-
³ He glass stem*	-	-	-0.61	0.20	-	-	-0.61	0.20
³ He cell rotation*	-	-	0	0.35			0	0.35
Sample magnetization	0	0	0	0.20	-93.10	0.26	0	0.18
Radiation damping*	-	-	0	0.18	-	-	0	0.18
$\sigma_p^{\rm H_2O}$ Temperature dependence	-0.48	0.64	-	-	-1.27	0.64	-	-
$\chi^{\rm H_2O}$ Temperature dependence	0	0	-	-	0	0.02	- 1	-
Total of corrections	12.84	1.60	20.77	1.31	- 77.65	1.62	23.05	1.23
Frequency extraction unc.	0.01		-		0.10		-	
Magnet drift uncertainty	0.05		0.09		0.18		0.12	
Position uncertainty*	0.07		0.05		0.07		0.05	
Total unc.	1.61		1.32		1.64		1.23	
$\omega'/2\pi$	61,710,229.90		47,009,998.24		61,715,758.45		47,014,209.45	
B-1,449,000,000 (nT)	400419 (41)		400448 (44)		530269(41)		530287 (42)	
$ R'_{hp} = \omega'_3/\omega'_p $	0.761786147 (29)			0.761786141 (28)				
Combined $ R'_{hp} $	0.761786144(20)							
$ \mu'_h (10^{-27} \text{ J T}^{-1})$	1.074553107(31)							

TABLE I: Corrections and uncertainties for cross-calibration studies of both $\rm H_2O$ probes. For entries with correction < 0.01 Hz, the correction, is indicated with a 0; entries that do not apply for a specific probe are indicated with a -.; the * indicates that one correction/uncertainty applies to both studies. The last two lines provide new determinations from this work to be compared to $|R'_{hp}| = 0.7617861313(33)$ and $|\mu'_{hp}| = 1.074553090(13) \times 10^{-27}$ J T⁻¹ based on [10]. To convert frequency uncertainties to approximate ppb, divide by 47.1×10^{-3} for ³He and 61.7×10^{-3} for $\rm H_2O$.

less than 1 mHz.

Effects of the FID frequency evolution due to dephasing in the non-uniform field are discussed by [45, 46]. Studies with simulated FIDs using the measured magnetic field gradients indicate that these effects were less than 0.1 Hz and less than 0.01 Hz for the cylindrical and spherical $\rm H_2O$ probes and negligible for $\rm ^3He$. Radiation damping shifts due to the current induced in the pickup coil was studied through the frequency-dependence of ω_3^{uncor} over a set of five 23° pulses. Extrapolating the the frequency dependence to zero longitudinal polarization sets an upper limit of 0.18 Hz on the shift. Radiation damping for the $\rm H_2O$ probes, studied by the longitudinal magnetization dependence over the five-pulse sequences and as the probe-tuning drifted, was negligible.

Temperature-dependence of the H₂O diamagnetic shielding was corrected to 25°C by measuring the temperature on the outside of the H₂O probe with a 1000Ω platinum resistor (PT1000). Conservatively estimating an uncertainty of 5 Ω corresponding to 1° resulted in 0.64 Hz uncertainty. From [47], $\chi^{\rm H_2O}$ was measured to change by 0.5% over 40°, which we interpret as $\partial \chi^{\rm H_2O}/\partial T = 1.1 \times 10^{-9}/^{\circ}\text{C}$, adding an uncertainty of 0.02 Hz for the H₂O cylindrical-probe shape correction.

Other Corrections and uncertainties including higherorder time dependence and field fluctuations, for example moving equipment or tools, was estimated as the standard deviation of the residuals of the linear fits in Fig 3. Clock stability was found to be better than 0.01 Hz. The position reproducibility was 0.2 mm (200 μ m) contributing an uncertainty 0.07 Hz for H₂O and 0.05 Hz for ³He.

Conclusions: The final results of measurements of the corrected frequencies and corresponding absolute magnetic field determined by the $^3{\rm He}$ and both ${\rm H_2O}$ probes are given in Table I. The absolute magnetic fields determined with $^3{\rm He}$ and ${\rm H_2O}$ differ by 20 ± 41 ppb and 12 ± 41 ppb for the spherical and cylindrical ${\rm H_2O}$ probes, respectively. Since the two ${\rm H_2O}$ probes with corrections consistent with those applied here [37] were used in the analysis of the E821 $g_\mu-2$ measurements [27, 28] this can be interpreted as confirming the calibration of the E821 magnetic-field measurement system to 16 ± 29 ppb, i.e. agreement better than 32 ppb (68% C.L.) compared to the 2.4 ppm tension of a_μ^{exp} from E821 with the Standard Model a_μ^{SM} .

We can also use the corrected frequencies to determine $|R'_{hp}| = |\mu'_h/\mu'_p(25^{\circ}\mathrm{C})|$ and $|\mu'_h| = |R'_{hp}||\mu'_p(25^{\circ})|$. The combined results for the two probes presented in Table I are consistent with [10] but with a 6.8 times larger error on $|R'_{hp}|$. (Both determinations of $|\mu'_h|$ use the shielded proton moment introducing a common uncertainty.) Straightforward improvements to the ³He magnetometer materials, structure, and improved measurement of the corrections should lead to determination of $|R'_{hp}|$ at the few ppb level and provide a new method for

absolute calibration of H₂O probes.

Most importantly, this work and improvements to our first-generation absolute $^3\mathrm{He}$ magnetometer establish the technical basis for practical absolute magnetometry with $^3\mathrm{He}$ and the establishment of a new magnetic field standard. Though this new standard would currently trace to measurements of μ_h'/μ_p' , the anticipated independent measurement of the helion moment [14] would provide a completely new magnetometry standard.

Acknowledgements We are grateful to Sam Henry and Babak Abi for contributions during the initial stages of development. This work was supported by NSF Grant Phy-1812314, DOE contract DE-AC02-06CH1135, and DOE grant DE-FG02-88ER40415.

- R. Körber et al., Superconductor Science and Technology 29, 113001 (2016).
- [2] D. Budker and M. V. Romalis, Nature Phys. 3, 227 (2007).
- [3] I. K. Kominis, T. W. Kornack, J. C. Allred, and M. V. Romalis, Nature 422, 596 (2003).
- [4] P. Arpaia, G. Caiafa, and S. Russenschuck, Scientific Reports 9, 1491 (2019).
- [5] Metrolab, https://www.metrolab.com.
- [6] W. Phillips, W. Cooke, and D. Kleppner, Metrologia 13, 179 (1977).
- [7] P. J. Mohr, D. B. Newell, and B. N. Taylor, Rev. Mod. Phys. 88, 035009 (2016), (2018 CODATA recommended values).
- [8] H. Koch, G. Bison, Z. Grujić, W. Heil, M. Kasprzak, P. Knowles, A. Kraft, A. Pazgalev, A. Schnabel, J. Voigt, and A. Weis, Eur. Phys. J. D 69, 262 (2015).
- [9] See Supplemental Material [url], which includes Refs. [48–68].
- [10] J. Flowers, B. Petley, and M. Richardson, Metrologia 30, 7 (1993).
- [11] Y. Neronov and N. Seregin, J. of Exp. and Theo. Phys. 115, 115 (2012).
- [12] B. Petley and R. Dondaldson, Metrologia 20, 21 (1984).
- [13] D. Sundholm, J. Gauss, and A. Schäfer, The Journal of Chemical Physics 105, 11051 (1996).
- [14] A. Mooser, A. Rischka, A. Schneider, K. Blaum, S. Ul-mer, and J. Walz, Journal of Physics: Conference Series 1138, 012004 (2018).
- [15] A. Schneider, A. Mooser, A. Rischka, K. Blaum, S. Ulmer, and J. Walz, Annalen der Physik 531, 1800485 (2019).
- [16] G. Schneider et al., Science 358, 1081 (2017).
- [17] C. Smorra et al., Nature 550, 371 (2017).
- [18] A. Rudzinski, M. Puchalski, and K. Pachucki, Journal of Chemical Physics 130, 244102 (2009).
- [19] P. A. M. Dirac, Proceedings of the Royal Society of London A: Mathematical, Physical and Engineering Sciences 117, 610 (1928).
- [20] J. Schwinger, Phys. Rev. **73**, 416 (1948).
- [21] T. Aoyama, T. Kinoshita, and M. Nio, Phys. Rev. D 97, 036001 (2018).
- [22] T. Aoyama, M. Hayakawa, T. Kinoshita, and M. Nio,

- Phys. Rev. Lett. 109, 111808 (2012).
- [23] M. Davier, A. Hoecker, B. Malaescu, and Z. Zhang, arXiv hep-ph, 1908.00921 (2019).
- [24] A. Keshavarzi, D. Nomura, and T. Teubner, arXiv hepph, 1911.00367 (2019).
- [25] J. Bailey *et al.* (CERN-Mainz-Daresbury), Nucl. Phys. B150, 1 (1979).
- [26] G. W. Bennett et al. (Muon g-2), Phys. Rev. D73, 072003 (2006).
- [27] G. W. Bennett et al. (Muon g-2), Phys. Rev. Lett. 89, 101804 (2002), [Erratum: Phys. Rev. Lett.89,129903(2002)].
- [28] G. W. Bennett et al. (Muon g-2), Phys. Rev. Lett. 92, 161802 (2004).
- [29] I. Logashenko *et al.* (Muon g-2), J. Phys. Chem. Ref. Data 44, 031211 (2015).
- [30] D. Hanneke, S. Fogwell and G. Gabrielse, Phys. Rev. Lett. 100, 120801 (2008).
- [31] W. Liu, M.G. Boshier, S. Dhawan, O. vanDyck, P. Egan, X. Fei, et al., Phys. Rev. Lett. 82, 711 (1999).
- [32] M. Abboud, A. Sinatra, X. Maître, G. Tastevin, and P.-J. Nacher, Europhysics Letters (EPL) 68, 480 (2004).
- [33] A. Nikiel, P. Blümler, W. Heil, M. Hehn, S. Karpuk, A. Maul, E. Otten, L. Schreiber, and M. Terekhov, Eur. Phys. J. D68, 330 (2014).
- [34] W. Heil, in *High Sensitivity Magnetometers*, Vol. 19, edited by A. Grosz, M. Haji-Sheikh, and S. Mukhopadhyay (Springer, Cham, Switzerland, 2017) pp. 493–521.
- [35] Keopsys.com Model CYFL-GIGA.
- [36] J. Maxwell, C. Epstein, and R. Milner, Nuc. Inst. and Meth. A764, 215 (2014).
- [37] X. Fei, V. W. Hughes, and R. Prigl, Nucl. Inst. and Meth. A394, 349 (1997).
- [38] M. Fertl, Fermilab E989 internal (2014).
- [39] J. H. Wesenberg and K. Mølmer, Phys. Rev. Lett. 93, 143903 (2004).
- [40] M. V. Romalis, D. Sheng, B. Saam, and T. G. Walker, Phys. Rev. Lett. 113, 188901 (2014).
- [41] D. Sheng, A. Kabcenell, and M. V. Romalis, Phys. Rev. Lett. 113, 163002 (2014).
- [42] M. E. Limes, N. Dural, M. V. Romalis, E. L. Foley, T. W. Kornack, A. Nelson, L. R. Grisham, and J. Vaara, Phys. Rev. A 100, 010501(R) (2019).
- [43] W. A. Terrano, J. Meinel, N. Sachdeva, T. E. Chupp, S. Degenkolb, P. Fierlinger, F. Kuchler, and J. T. Singh, Phys. Rev. A 100, 012502 (2019).
- [44] N. Sachdeva, I. Fan, E. Babcock, M. Burghoff, T. E. Chupp, S. Degenkolb, *et al.*, Phys. Rev. Lett. **123**, 143003 (2019).
- [45] J. Flowers, P. Franks, and B. Petley, IEEE Trans. on Inst. and Meas. 44, 488 (1995).
- [46] B. Cowan, Meas. Sci. and Tech. 7, 690 (1996).
- [47] J. S. Philo and W. M. Fairbank, J. of Chem. Phys. 72, 4429 (1980).
- [48] S. G. Karshenboim and V. G. Ivanov, Phys. Lett. B566, 27 (2003).
- 49 Y. I. Neronov and N. Seregin, Metrologia 51, 54 (2014).
- [50] N. Nevo Dinur, O. J. Hernandez, S. Bacca, N. Barnea, C. Ji, S. Pastore, M. Piarulli, and R. B. Wiringa, Phys. Rev. C 99, 034004 (2019).
- [51] M. A. Bouchiat, T. R. Carver, and C. M. Varnum, Phys. Rev. Lett. 5, 373 (1960).
- [52] T. E. Chupp and K. P. Coulter, Phys. Rev. Lett. 55, 1074 (1985).

- [53] F. D. Colegrove, L. D. Schearer, and G. K. Walters, Phys. Rev. Lett. 8, 439 (1962).
- [54] T. R. Gentile, P. J. Nacher, B. Saam, and T. G. Walker, Rev. Mod. Phys. 89, 045004 (2017).
- [55] K. Coulter *et al.*, Nucl. Inst. and Meth. in Phys. Res. A 288, 463 (1990).
- [56] E. Babcock *et al.*, Journal of Physics: Conference Series 711, 012008 (2016).
- [57] T. E. Chupp, R. A. Loveman, A. K. Thompson, A. M. Bernstein, and D. R. Tieger, Phys. Rev. C45, 915 (1992).
- [58] A. Camsonne et al., Phys. Rev. Lett. 119, 162501 (2017).
- [59] T. E. Chupp, P. Fierlinger, M. J. Ramsey-Musolf, and J. T. Singh, Rev. Mod. Phys. 91, 015001 (2019).
- [60] D. Bear, R. E. Stoner, R. L. Walsworth, V. A. Kostelecky, and C. D. Lane, Phys. Rev. Lett. 85, 5038 (2000), [Erratum: Phys. Rev. Lett. 89, 209902(E) (2002)].

- [61] R. Surkau et al., Nuc. Inst. and Meth. A384, 444 (1997).
- [62] F. Allmendinger, W. Heil, S. Karpuk, W. Kilian, A. Scharth, U. Schmidt, A. Schnabel, Yu. Sobolev, and K. Tullney, Phys. Rev. Lett. 112, 110801 (2014).
- [63] J. M. Wild et al., Physics in Medicine and Biology 47, N185 (2002).
- [64] J. Mulger and T. Altes, J. Magn. Reson. Imaging 37, 313 (2013).
- [65] G. D. Cates, S. R. Schaefer, and W. Happer, Phys. Rev. A37, 2877 (1988).
- [66] D. D. McGregor, Phys. Rev. A 41, 2631 (1990).
- [67] T. E. Chupp, R. J. Hoare, R. L. Walsworth, and B. Wu, Phys. Rev. Lett. 72, 2363 (1994).
- [68] Y. Chibane, S. K. Lamoreaux, J. M. Pendlebury, and K. F. Smith, Measurement Science and Technology 6, 1671 (1995).